Autism-linked neuroligin-3 R451C mutation differentially alters hippocampal and cortical synaptic function

Mark Etherton[a,1], Csaba Földy[a], Manu Sharma[a], Katsuhiko Tabuchi[a,2], Xinran Liu[b], Mehrdad Shamloo[c], Robert C. Malenka[d], and Thomas C. Südhof[a,b,d,e,f,3]

[a]Department of Molecular and Cellular Physiology, Stanford University Medical School, Stanford, CA 94305; [b]Department of Neuroscience, University of Texas Southwestern Medical Center, Dallas, TX 75390; [c]Behavioral and Functional Neuroscience Laboratory, Stanford Institute for Neuro-Innovation and Translational Neurosciences, Stanford University Medical School, Stanford, CA 94305; [d]Nancy Pritzker Laboratory, Department of Psychiatry, Stanford University Medical School, Stanford, CA 94305; [e]Howard Hughes Medical Institute, Stanford University Medical School, Stanford, CA 94305; and [f]Howard Hughes Medical Institute, University of Texas Southwestern Medical Center, Dallas, TX 75390

Contributed by Thomas C. Südhof, July 11, 2011 (sent for review June 23, 2011)

Multiple independent mutations in neuroligin genes were identified in patients with familial autism, including the R451C substitution in neuroligin-3 (NL3). Previous studies showed that NL3^{R451C} knock-in mice exhibited modestly impaired social behaviors, enhanced water maze learning abilities, and increased synaptic inhibition in the somatosensory cortex, and they suggested that the behavioral changes in these mice may be caused by a general shift of synaptic transmission to inhibition. Here, we confirm that NL3^{R451C} mutant mice behaviorally exhibit social interaction deficits and electrophysiologically display increased synaptic inhibition in the somatosensory cortex. Unexpectedly, however, we find that the NL3^{R451C} mutation produced a strikingly different phenotype in the hippocampus. Specifically, in the hippocampal CA1 region, the NL3^{R451C} mutation caused an ∼1.5-fold increase in AMPA receptor-mediated excitatory synaptic transmission, dramatically altered the kinetics of NMDA receptor-mediated synaptic responses, induced an approximately twofold up-regulation of NMDA receptors containing NR2B subunits, and enhanced long-term potentiation almost twofold. NL3 KO mice did not exhibit any of these changes. Quantitative light microscopy and EM revealed that the NL3^{R451C} mutation increased dendritic branching and altered the structure of synapses in the stratum radiatum of the hippocampus. Thus, in NL3^{R451C} mutant mice, a single point mutation in a synaptic cell adhesion molecule causes context-dependent changes in synaptic transmission; these changes are consistent with the broad impact of this mutation on murine and human behaviors, suggesting that NL3 controls excitatory and inhibitory synapse properties in a region- and circuit-specific manner.

synapse formation

Autism spectrum disorders (ASDs) constitute a heterogeneous group of neurodevelopmental diseases with a strong genetic component (1–3). The identification of multiple ASD candidate genes that encode synaptic proteins suggested that ASDs may involve impairments in synaptic transmission (4–12). In particular, numerous mutations in neuroligins, a family of postsynaptic cell adhesion molecules, have been identified in ASDs (4–7, 10, 12). Consistent with the hypothesis that synaptic dysfunction contributes to ASD pathogenesis (13, 14), mouse models of two ASD-associated neuroligin mutations exhibit functional changes in synaptic transmission (15, 16).

Neuroligins are not critical for the initial establishment of synapses but are required for normal synapse function (17–20). Deletion of neuroligin-1 or -2 selectively impairs excitatory or inhibitory synaptic transmission, respectively (17, 18, 21, 22), whereas at least in the somatosensory cortex, deletion of neuroligin-3 (NL3) causes no major synaptic phenotype (15). Three ASD-relevant neuroligin mutations were characterized in mouse models: the R451C substitution in NL3 (15, 23), a loss of function mutation of NL4 (24), and a point mutation that was identified in the cytoplasmic tail of NL4 in an ASD patient but was analyzed in the context of NL3 (16). Characterization of NL3^{R451C} knock-in mice uncovered a behavioral phenotype composed of social interaction deficits and increased spatial memory and an electrophysiological phenotype consisting of increased inhibitory synaptic transmission in the somatosensory cortex (15). However, an independently generated second line of NL3^{R451C} mutant mice exhibited a different behavioral phenotype, although the physiological phenotype was not tested (23). Because behavioral properties of mice are background-dependent, differences in behavioral phenotypes between mouse lines are not surprising, but physiological properties of synapses are thought to be background-independent, raising the question of whether the two NL3^{R451C} mutant mouse lines exhibit similar synaptic changes. In more general terms, ASD pathogenesis likely involves multiple brain areas, prompting the more important question of whether the NL3^{R451C} mutation has similar or different effects on synaptic transmission in different brain regions and neuronal circuits. Thus, at present, two major questions emerge. First, does the NL3^{R451C} mutation cause the same changes in synaptic transmission in different mouse lines, and second and more importantly, does the NL3^{R451C} mutation change synaptic transmission similarly in all brain regions or act in a circuit-dependent, brain region-specific fashion?

To address these questions, we have here reassessed the behavioral and physiological effects of the NL3^{R451C} mutation in mice. In the physiological studies, we focused on the CA1 region of the hippocampus, which is arguably the best-studied brain area of the mammalian forebrain and among many other behaviors, has also been implicated in sociability (25). Strikingly, we find that the NL3^{R451C} mutation, as assessed in both of the two independently generated mouse lines, caused a large increase in AMPA and NMDA receptor-mediated excitatory synaptic transmission and a dramatic change in NMDA receptor-mediated responses in the hippocampus, whereas the same mutation selectively increased inhibitory synaptic transmission in the somatosensory cortex. Thus, the NL3^{R451C} mutation induces general context-specific alterations in synaptic function that re-

Author contributions: M.E., C.F., X.L., M.Shamloo, R.C.M., and T.C.S. designed research; M.E., C.F., M.Sharma, K.T., X.L., and M.Shamloo performed research; M.E., C.F., M.Sharma, K.T., X.L., M.Shamloo, and T.C.S. analyzed data; and M.E., C.F., X.L., M.Shamloo, R.C.M., and T.C.S. wrote the paper.

The authors declare no conflict of interest.

[1]Present address: Medical Scientist Training Program, University of Texas Southwestern Medical Center, Dallas, TX 75390.

[2]Present address: Department of Cerebral Research, National Institute for Physiological Sciences, Okazaki 444-8787, Japan.

[3]To whom correspondence should be addressed. E-mail: tcs1@stanford.edu.

This article contains supporting information online at www.pnas.org/lookup/suppl/doi:10.1073/pnas.1111093108/-/DCSupplemental.

sult in region-specific changes in neural circuits with accompanying alterations in ASD-relevant mouse behaviors.

Results

NL3^{R451C} Mutation Impairs Social Interactions. Because deficits in social interaction represent one of the core criteria for diagnosis of ASDs, we reevaluated social behaviors in NL3^{R451C} mutant mice. Previous analyses of social behaviors in NL3^{R451C} mutant mice provided conflicting results (15, 23), prompting us to reassess the sociability of NL3^{R451C} mutant mice in a different behavioral facility and institution using a three-chamber test (26–28). In this test, the subject mouse is first habituated to the testing environment (habituation session), then exposed to a novel mouse in one of the target chambers and a novel object in the opposite chamber (sociability session), and finally, tested for preference for social novelty by replacing the no longer novel object in the opposite chamber with a new unfamiliar mouse.

In the initial habituation session, littermate NL3^{R451C} mutant and WT mice did not exhibit a side preference for the left or right chamber. During the subsequent sociability session, both NL3^{R451C} mutant mice and WT control mice displayed a significant preference for the cage containing the stranger mouse (Fig. 1*A*). During the final social novelty session, WT mice spent significantly more time sniffing at the novel stranger than at the now-familiar social object, whereas NL3^{R451C} mutant mice did not (Fig. 1*A*).

To further examine the sociability phenotype observed in the three-chamber test, NL3^{R451C} mutant mice were tested in a caged adult social interaction test (15). In this task, NL3^{R451C} mutant mice showed no change in the time of interaction with a novel inanimate object in the first phase of this test (Fig. 1 *B* and *C*). During the second phase of this test, however, mutant mice explored the unfamiliar caged mouse significantly less than WT controls during the entire time course of the second trial (Fig. 1*B*) (effect of genotype; $F_{1,\ 306} = 4.47$, $P = 0.042$). In addition, the mutant mice displayed a decreased time of interaction with the target mice during the total trial (Fig. 1*C*). Thus, two tests confirm a modest but significant social interaction deficit in NL3^{R451C} mutant mice.

NL3^{R451C} Mutation Increases AMPA Receptor-Mediated Synaptic Transmission in the CA1 Region of the Hippocampus. To examine the effect of the NL3^{R451C} mutation on synaptic transmission in other brain regions than the somatosensory cortex (15), we performed extracellular field recordings in the CA1 region of the hippocampus and additionally, analyzed NL3 KO mice in parallel. We plotted the slope of the field excitatory postsynaptic potential (fEPSP; mediated primarily by AMPA-type glutamate receptors) relative to the number of afferents stimulated, which was measured by the fiber volley amplitude. Input–output measurements using this approach showed that the NL3^{R451C} mutation unexpectedly caused a large increase in excitatory synaptic transmission, whereas the NL3 KO had no effect (Fig. 2 *A*–*C*). To ensure that this effect was a direct effect of the NL3^{R451C} mutation, we also analyzed the independently generated NL3^{R451C} mutant mouse line (23) (referred to as R451C*) and observed the same phenotype (Fig. 2*C*). The observation that this synaptic change is reproducible in two independently generated lines of NL3^{R451C} mutant mice but is absent from NL3 KO mice indicates that the enhancement of AMPA receptor-mediated synaptic transmission in the hippocampus represents a core effect of the NL3^{R451C} mutation. Moreover, this effect is not caused by changes in presynaptic release probability, which was assessed by paired-pulse facilitation experiments (Fig. S1).

NL3^{R451C} Mutation Enhances NMDA Receptor-Mediated Hippocampal Synaptic Transmission. To further characterize the effects of the NL3^{R451C} mutation on excitatory synaptic transmission, we analyzed the ratio of synaptic transmission mediated by NMDA- vs. AMPA-type glutamate receptors (the NMDA/AMPA ratio) in CA1 region pyramidal neurons (Fig. 3*A*). The NMDA/AMPA ratio was significantly increased in the hippocampus in NL3^{R451C} mutant mice but was unchanged in NL3 KO mice (Fig. 3*B*). Conversely, the NMDA/AMPA ratio was not significantly altered by the NL3^{R451C} mutation in layer 2/3 pyramidal neurons of the somatosensory cortex (Fig. 3 *A* and *B*). Analysis of the independently generated NL3^{R451C} mutant mouse line (23) confirmed the increase in NMDA/AMPA ratio in the hippocampus (Fig. 3*B*). Because the input–output measurements (Fig. 2) showed that the NL3^{R451C} mutation enhances AMPA receptor-mediated synaptic transmission, the enhanced NMDA/AMPA ratio implies that NMDA receptor-mediated transmission is increased in NL3^{R451C} mutant mice to an even greater extent than AMPA receptor-mediated transmission.

The results obtained in the hippocampus differ dramatically from those results described for the somatosensory cortex, where an increase in spontaneous and evoked inhibitory synaptic transmission was detected (15). To reassess whether the NL3^{R451C} mutation produces circuit-specific alterations of synaptic transmission, we directly compared spontaneous miniature synaptic events in acute slices from the hippocampus and somatosensory cortex of NL3^{R451C} mutant and NL3 KO mice (Fig. S2). The NL3^{R451C} mutation produced a significant increase in the frequency of spontaneous miniature excitatory postsynaptic currents (mEPSCs) in the hippocampus without a change in

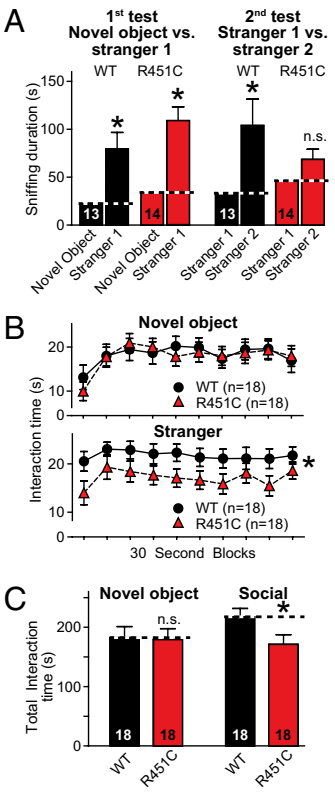

Fig. 1. NL3^{R451C} knock-in mice exhibit social interaction impairments. (*A*) Three-chamber sociability test. Mice were first simultaneously exposed to an empty round wire container (pencil cup) as a novel object and a caged, unfamiliar mouse (*Left*). Afterward, a novel mouse was introduced into the empty wire container (*Right*). The sniffing duration for each mouse was measured as shown (paired *t* test; *Left*: WT = $P < 0.01$, R451C = $P < 0.0001$; *Right*: WT = $P < 0.05$, R451C = n.s.). (*B*) Caged adult social interaction test. Mice were sequentially exposed to a novel object (empty rectangular wired cage) and a caged stranger mouse, and the time course of interaction was measured in 30-s time bins. No differences in the genotype were detected during the novel object interaction trial (*Upper*) but were measured during the social trial (*Lower*; effect of genotype: $F_{1,\ 306} = 4.47$, $P = 0.042$). (*C*) Summary graphs of the total interaction time measured in *B*. (*$P < 0.05$ by unpaired *t* test; n.s. = nonsignificant). Data represent means ± SEMs.

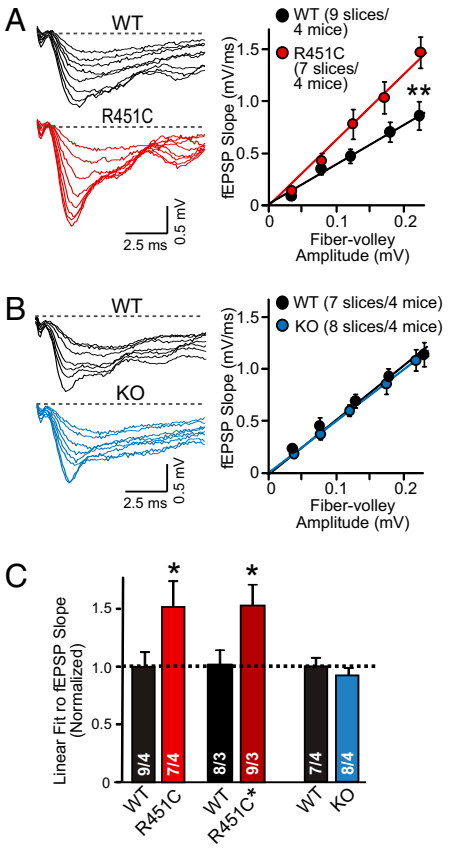

Fig. 2. NL3^{R451C} knock-in mutation increases excitatory synaptic transmission in the CA1 region of the hippocampus. (*A*) Representative traces and summary graph of input–output measurements performed by extracellular field recordings in acute hippocampal slices from littermate WT and NL3^{R451C} mutant mice (R451C). (*B*) Same as *A*, except that NL3 KO mice were analyzed. (*C*) Summary graph of the linear slope fits measured during input–output recordings for NL3 KO and NL3^{R451C} mutant mice. Note that two independent lines of NL3^{R451C} mutant mice were examined (the lines described by Tabuchi et al. in ref. 15, referred to as R451C, and Chadman et al. in ref. 23, referred to as R451C*) in addition to the NL3 KO mice. Data represent means ± SEMs. Statistical significance ($P < 0.01$) was evaluated with one-way ANOVA (*A* and *B*) or Student *t* test (*C*). Total number of slices and mice examined are shown in the bars of panel *C*. Paired-pulse measurements are in Fig. S1.

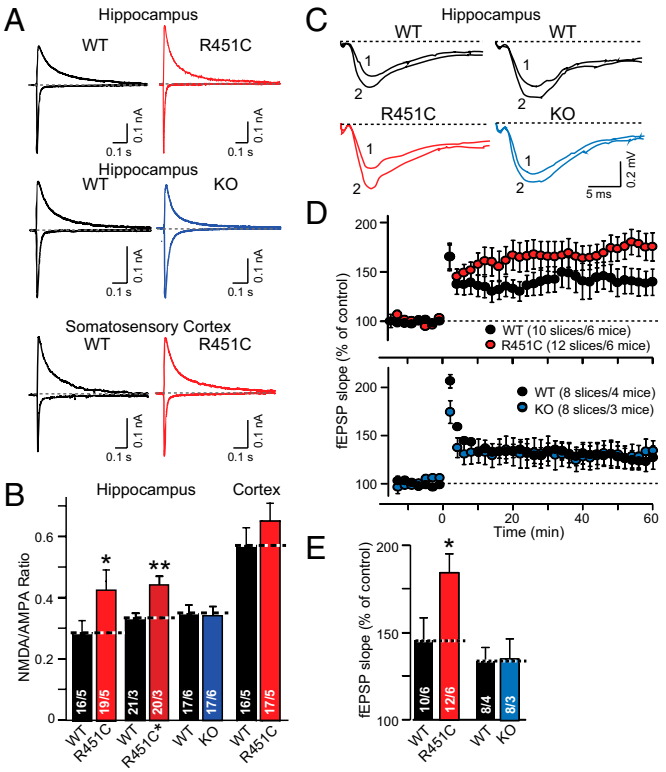

Fig. 3. NL3^{R451C} knock-in mutation increases NMDA receptor-mediated synaptic responses and LTP in the hippocampus. (*A*) Sample traces of measurements of the ratio of NMDA vs. AMPA receptor-mediated synaptic currents. Analyses compared littermate WT and NL3^{R451C} mutant mice in the hippocampus and layer 2/3 of the somatosensory cortex and littermate WT and NL3 KO mice in the hippocampus as indicated. AMPA and NMDA receptor-mediated responses were monitored with postsynaptic holding potentials of −70 and +40 mV, respectively. (*B*) Summary graphs of the NMDA/AMPA receptor response ratios as indicated. Note that, as in Fig. 1, two independent lines of NL3^{R451C} mutant mice were examined [in Tabuchi et al. (15), mice were referred to as R451C, and in Chadman et al. (23), mice referred to as R451C*]. Parallel measurements of spontaneous release are in Fig. S2. (*C*) Sample traces from extracellular field recordings performed in the CA1 region in acute slices of the hippocampus from littermate WT and NL3^{R451C} mutant (*Left*) or WT and NL3 KO mice (Right). LTP was induced by three 1-s, 100-Hz stimulations. Traces are from before (1) or 60 min after LTP induction (2). (*D*) Summary graphs of the fEPSP slope as a function of LTP induction monitored in acute slices from WT and mutant mice as indicated. (*E*) Plot of the average percentage of synaptic transmission increase during LTP measured 55–60 min postinduction relative to baseline. Data represent means ± SEM; in *B* and *E*, total numbers of cells or slices/total number of mice are indicated in the bars, respectively. Statistical significance was evaluated with Student *t* test (*$P < 0.05$; **$P < 0.01$).

miniature inhibitory postsynaptic currents (mIPSCs) but an increase in mIPSCs in the somatosensory cortex without a change in mEPSCs. These results confirm the circuit specificity of the NL3^{R451C} mutant phenotype and agree with the above findings that the NL3^{R451C} mutation enhances AMPA receptor-mediated synaptic transmission (Fig. S2). In addition, the mini recordings uncovered the only phenotype in NL3 KO mice that we detected in the current study, namely a decrease in mEPSC frequency in the hippocampus, which is opposite of the increase caused by the NL3^{R451C} mutation, and an increase in the mIPSC frequency (Fig. S2).

Enhanced Long-Term Potentiation (LTP) in NL3^{R451C} Mutant Mice. The increased NMDA/AMPA ratio observed in NL3^{R451C} mutant mice led us to hypothesize that NL3^{R451C} mutant mice may have enhanced NMDA receptor-dependent LTP in the CA1 region of the hippocampus, a finding that could partly explain the increased spatial memory observed in these mice (15). To test this hypothesis, we assessed LTP in response to three stimulus trains (100 Hz for 1 s) using extracellular field recordings (Fig. 3*C*). Indeed, NL3^{R451C} mutant mice exhibited significantly enhanced LTP (Fig. 3*D*). Quantitation of the degree of LTP at 55–60 min after induction showed an ∼70% increase in NL3^{R451C} mutant mice, whereas LTP in NL3 KO mice was unchanged (Fig. 3*E*).

NL3^{R451C} Mutation Alters the Synaptic NMDA Receptor Subunit Composition in the Hippocampus. The increased NMDA receptor-mediated synaptic transmission in the hippocampus from NL3^{R451C} mutant mice could be because of either an increase in the number of NMDA receptors and/or a change in the NMDA receptor subunit composition, resulting in higher conductances (29, 30). We, thus, characterized the properties of NMDA receptors in NL3^{R451C} mutant mice. The NMDA receptor current–voltage relationship was normal in NL3^{R451C} mutant mice, implying that there is no change in the Mg^{2+} sensitivity of NMDA receptors (Fig. 4*A*). Interestingly, the decay time constant of NMDA receptor-mediated responses at +40 mV was significantly increased (Fig. 4*B*), suggesting a shift in NMDA

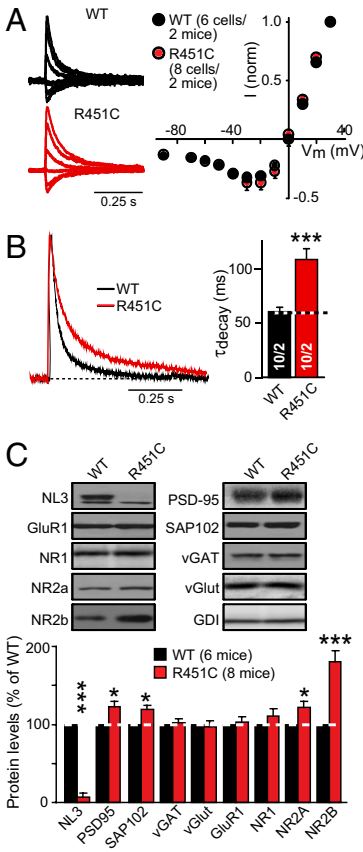

Fig. 4. $NL3^{R451C}$ mutation alters kinetics and composition of synaptic NMDA receptors. (*A*) Normalized sample traces (*Left*) and summary graph (*Right*) for NMDA receptor current voltage measurements. (*B*) Normalized sample traces (*Left*) and summary graph (*Right*) for NMDA receptor decay kinetics measurements. (*C*) Representative immunoblots of the indicated proteins (*Upper*) and total protein levels in hippocampal lysates measured using quantitative immunoblotting with ^{125}I-labeled antibodies and phosphoImager detection (*Lower*). Hippocampal lysates were from littermate WT and $NL3^{R451C}$ knock-in mice at 6 wk of age. Protein levels were normalized first to GDP-dissociation inhibitor (GDI) as an internal loading control and then, to WT levels. Data shown are means ± SEMs (*$P < 0.05$; ***$P < 0.001$ using Student *t* test; in *B*, total number of cells/total number mice analyzed are shown in the bar diagrams).

receptor subunit composition (29, 30), with the most likely explanation being a switch from NR2A-type subunit to NR2B-type subunit containing NMDA receptors.

To probe this possibility, we measured the levels of selected synaptic proteins in the hippocampus by quantitative immunoblotting (Fig. 4*C*). Consistent with previous reports (15, 23), the $NL3^{R451C}$ mutation significantly reduced NL3 protein levels and had no effect on most synaptic proteins, including AMPA receptors. However, the $NL3^{R451C}$ mutation increased the concentrations of excitatory postsynaptic scaffolding proteins (PSD-95 and SAP-102) and doubled the concentration of the NMDA receptor subunit NR2B (Fig. 4*C*). No change in other synaptic proteins, particularly proteins specific for inhibitory synapses, was observed (Fig. S3*C*).

To further test whether the $NL3^{R451C}$ mutation alters postsynaptic glutamate receptor composition, we pharmacologically isolated the different components of NMDA receptor-mediated responses using ifenprodil, a selective antagonist of NR1/NR2B heterotetrameric NMDA receptors (31). In $NL3^{R451C}$ mutant mice, the ifenprodil sensitivity of NMDA receptor-mediated EPSCs was greater than in WT controls (Fig. S3), consistent with the hypothesis that the enhanced NMDA/AMPA ratio is, at least in part, secondary to a relative up-regulation of synaptic NR2B-containing NMDA receptors in CA1 pyramidal neurons. Thus, both the electrophysiological and biochemical results suggest that the $NL3^{R451C}$ mutation alters the synaptic NMDA receptor subunit composition, resulting in enhanced expression of NR2B-containing receptors.

$NL3^{R451C}$ Mutant Pyramidal Neurons Exhibit Changes in Synapse Structure and Dendritic Complexity. Although previous studies in the somatosensory cortex failed to uncover major morphological changes in $NL3^{R451C}$ mutant neurons (15), subtle structural alterations may have been missed. To assess the structure of dendrites in $NL3^{R451C}$ mutant neurons, we performed Sholl analyses on biocytin-filled CA1 pyramidal neurons. Interestingly, we found that $NL3^{R451C}$ mutant pyramidal neurons had a significantly greater number of dendritic branch points in the stratum radiatum but not in the stratum oriens or stratum lacunosum moleculare (Fig. 5 *A* and *B* and Fig. S4). The density of spines on secondary dendrites, however, was unchanged (Fig. 5*C*), suggesting that, overall, the neurons contain more synapses in the stratum radiatum; this finding is in agreement with the observed increase in AMPA receptor-mediated synaptic transmission.

To further assess the phenotype of the $NL3^{R451C}$ mutation, we examined by EM the structure of excitatory synapses in the stratum radiatum of $NL3^{R451C}$ mutant mice (Fig. 5*D*). We observed no major changes in the size of the postsynaptic density or number of docked vesicles in $NL3^{R451C}$ mutant mice (Fig. 5 *E* and *F*), but we detected significant reductions in spine area, bouton area, and total number of vesicles per bouton (Fig. 5 *G–I*). Thus, the $NL3^{R451C}$ mutation increases dendritic branching in the stratum radiatum of the CA1 region of the hippocampus without changing the density of synapses per branch length and renders the size, but not the junctional complex of synapses, significantly smaller.

Discussion

In the present study, we show that a single point mutation in NL3, the $NL3^{R451C}$ mutation that was associated with highly penetrant autism in a Swedish family (4), alters synaptic function in a circuit-dependent manner. Specifically, our findings are consistent with the following conclusions:

i) The $NL3^{R451C}$ mutant phenotype differs dramatically from the phenotype of the NL3 KO, suggesting that, despite the destabilization of NL3 protein by the R451C mutation that causes a loss of most NL3 protein (Fig. 4*C*), the remaining ~10% of $NL3^{R451C}$ mutant protein exerts a powerful gain of function effect on synaptic transmission.

ii) The $NL3^{R451C}$ mutation induces distinct phenotypes in the CA1 region of the hippocampus and layer 2/3 of the somatosensory cortex. In the former, it causes an enhancement of excitatory synaptic transmission and a change in the glutamate receptor composition of synapses; in the latter, it produces an enhancement of inhibitory synaptic transmission. Thus, the $NL3^{R451C}$ mutation does not act by the same mechanism in all synapses, but its effects are dependent on the synaptic context.

iii) In the CA1 region of the hippocampus, the $NL3^{R451C}$ mutation not only increased AMPA receptor-mediated synaptic transmission but also enhanced NMDA receptor-mediated transmission to an even larger degree, and it altered the subunit composition of postsynaptic NMDA receptors (Figs. 2–4). This finding suggests that the $NL3^{R451C}$ mutation not only increases synaptic transmission in a context-dependent fashion but also changes the properties of the affected synapses.

iv) Morphologically, the $NL3^{R451C}$ mutation enhanced the complexity of dendritic branching in the stratum radiatum of the hippocampal CA1 region (Fig. 5 *A* and *B*), thereby likely increasing synapse numbers and accounting for the increased excitatory synaptic transmission (Fig. 2 and Fig.

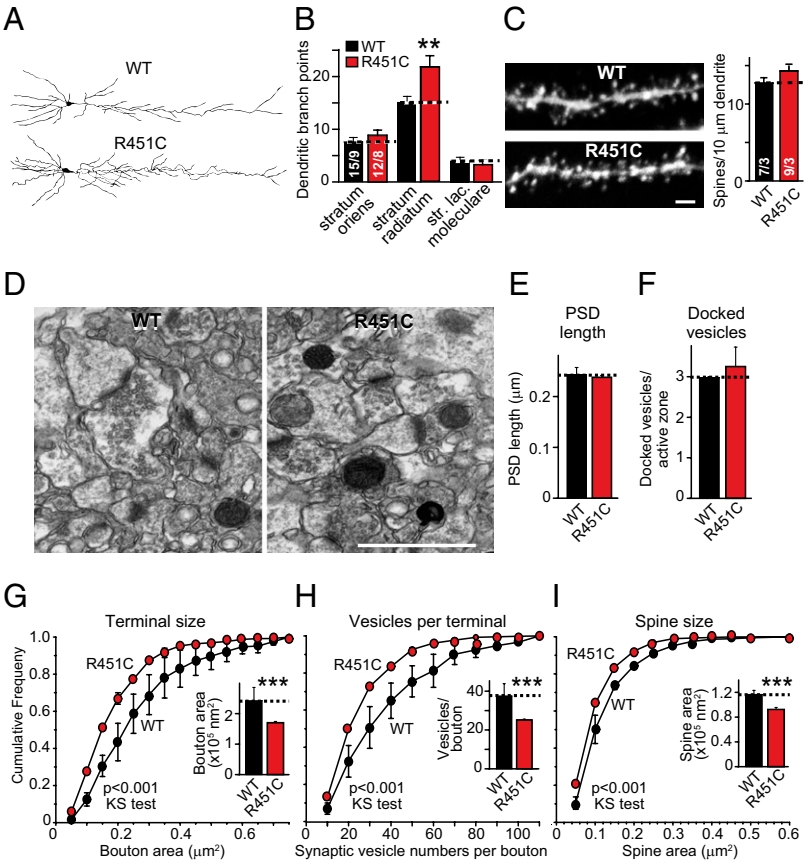

Fig. 5. Changes in dendritic branching and synapse structure in NL3^{R451C} mutant stratum radiatum of the CA1 region of the hippocampus. (*A* and *B*) Representative images (*A*) and summary graph of the number of dendritic branch points (*B*) of biocytin-filled pyramidal neurons in the CA1 region of the hippocampus. Neurons were filled with biocytin through a patch pipette in acute slices (str. lac. molecular, stratum lacunosum moleculare). (*C*) Representative images and summary graph of the spine density of dendrites in the stratum radiatum of Alexa-555–filled pyramidal neurons in the CA1 region of the hippocampus. (Scale bar: 1.985 µm.) (*D*) Representative electron micrographs from the stratum radiatum of the CA1 region of the hippocampus. (Scale bar: 1 µm.) (*E* and *F*) Summary graph of PSD size and number of docked vesicles in excitatory synapses of the stratum radiatum of the CA1 region of the hippocampus from littermate WT and NL3^{R451C} mutant mice. (*G–I*) Quantitation of the presynaptic nerve terminal size (*G*), number of vesicles per terminal (*H*), and spine size (*I*) in excitatory synapses of the stratum radiatum of the CA1 region from littermate WT and NL3^{R451C} mutant mice. Data represent means ± SEM. For *B* and *C*, numbers in bars indicate numbers of neurons/mice analyzed; for *E–I*, 303 electron micrographs from two pairs of littermates with 552 (WT) and 778 synapses (R451C) were measured. Statistical significance was evaluated by Student *t* test (*P < 0.05; **P < 0.01; ***P < 0.001).

S2). In NL3^{R451C} mutant mice, the synapses in the stratum radiatum contain a relatively higher content of NR2B-type NMDA receptors (Fig. 4 *B* and *C* and Fig. S3), are morphologically smaller (Fig. 5 *G–I*), and exhibit greater LTP (Fig. 3 *C–E*). However, postsynaptic density (PSD) length and mEPSC amplitudes are normal. Thus, in the stratum radiatum, the NL3^{R451C} mutation delays specific components of normal synaptic maturation while simultaneously increasing dendritic complexity.

A potential concern with a germline mutation introduced into mice by homologous recombination is that additional genetic changes are induced that may cause unrelated phenotypes. This concern was raised for the NL3^{R451C} mutation, because different behavioral phenotypes were reported for two independently generated mouse lines (15, 23). However, we show here that, in two key electrophysiological tests, two independent mouse lines exhibit the same phenotype, suggesting that this phenotype truly reflects a functional change induced by the NL3^{R451C} mutation.

The molecular basis of the NL3^{R451C} mutant phenotype and its circuit specificity remains unclear. The circuit specificity of the phenotype suggests that the NL3^{R451C} mutant protein does not produce the phenotype by interactions with canonical building blocks of all synapses—in which case, the phenotype should be similar in all neurons—but that its effect is dependent on the local protein environment unique to a particular synapse. Because in situ hybridizations indicate that NL3 is expressed in all brain regions and all neurons (17) (www.brain-map.org), it seems unlikely that the region specificity of the NL3^{R451C} mutant phenotype is caused by region-specific NL3 expression patterns. Instead, it seems reasonable that the differential expression of NL3 ligands (known and unknown) is responsible for this phenotype. In support of this hypothesis, distinct region-specific expression patterns have been shown for neurexin isoforms and splice variants (32, 33). Moreover, other NL3 ligands likely contribute to NL3 function (20) and may also participate in the NL3^{R451C} mutant phenotype; identification of such ligands will be required to clarify this issue.

The NL3^{R451C} mutation was identified in a family with two affected sons with ASDs whose mutation was inherited from an asymptomatic heterozygous mother (4). The dramatic circuit-specific effects of the NL3^{R451C} mutation on synaptic transmission could account for the diverse and variable symptoms observed in ASDs, which include not only impairments in social communication but also stereotypic behaviors, restricted interests, seizures, and changes in cognitive abilities ranging from common mental retardation to rare improvements in spatial or mathematical abilities. Genetic background effects and developmental influences likely differentially shape synaptic properties in different brain regions; in fact, the two autistic brothers carrying the NL3^{R451C} mutation exhibited significant clinical heterogeneity: one brother had classical autism, whereas the other had Asperger's syndrome (4). The pervasive but distinct synaptic phenotype produced by the NL3^{R451C} mutation in different brain regions suggests that the diverse clinical spectrum of ASD pathologies is secondary to region-specific susceptibilities that are modulated by genetic background effects and developmental or environmental influences.

Experimental Procedures

Mouse Husbandry and Genotyping. Mice were genotyped as described (15). All animal protocols and husbandry practices were approved by the Institutional Animal Care and Use Committee at Stanford University. All experiments were performed on littermate WT and mutant male mice.

Behavioral assays were performed using an established three-chamber sociability and social novelty test (26–28) and a caged adult social interaction text (15) as described in detail in *SI Text*.

Electrophysiology recordings were performed as described (15, 31) using acute slices from littermate WT or NL3^{R451C} mutant mice (P28-40; details in *SI*

Text). Extracellular field recordings were performed in 50 μM picrotoxin using patch pipettes (2–4 MΩ) filled with artificial cerebrospinal fluid and stimulation rates of 0.1 Hz (34). Whole-cell voltage-clamp recordings were performed with excitatory (117.5 mM $CsMeSO_4$, 10 mM Hepes, 10 mM tetraethylammonium chloride (TEA-Cl), 15.5 mM CsCl, 1 mM $MgCl_2$, 10 mM Na-phosphocreatine, 8 mM NaCl, 0.3 mM NaGTP, 4 mM MgATP, 5 mM EGTA, 1 mM QX-314) or inhibitory specific (120 mM CsCl, 10 mM Hepes, 5 mM NaCl, 1 mM $MgCl_2$, 0.3 mM NaGTP, 3 mM MgATP, 10 mM EGTA, 5 mM QX-314) internal pipette solutions in artificial cerebrospinal fluid containing 50 μM picrotoxin (for recording excitatory events) or 10 μM 2,3-Dioxo-6-nitro-1,2,3,4-tetrahydrobenzo[*f*]quinoxaline-7-sulfonamide (NBQX) (Tocris) and 50 μM AP5 (Tocris) (for recording inhibitory events). CA1 pyramidal neurons and layer 2/3 pyramidal neurons were patched based on their morphology and location. mEPSC/mIPSC recordings were performed in the presence of 0.5 mM tetrodotoxin (TTX) (31). NMDA/AMPA receptor ratios were analyzed in two steps for each neuron. First, stable synaptic responses were obtained at −70 mV (the amplitude of these responses was the AMPA-R–specific component); next, the holding potential was changed to +40 mV, and dual component EPSCs were collected. At 50 ms poststimulus, when the AMPA-R contribution was negligible, the amplitude of the dual component EPSC was interpreted as the NMDA-R–specific component. For NMDA/AMPA experiments in layer 2/3 pyramidal neurons, a stimulating electrode was placed in layer 1 of the somatosensory cortex. Extracellular LTP experiments were performed as described previously (35). NMDA receptor current/voltage relationships were examined in 50 μM picrotoxin and 10 μM NBQX with 5–10 traces at each holding potential. For NMDA receptor decay kinetics, at least 40 traces were averaged at +40 mV. The EPSC decay time constants were determined as the average-weighted mean of time constants in a double exponential fit. Ifenprodil experiments were performed in two stages. Stable NMDA-mediated responses were established at +40 mV for at least 3 min; then, 5 μM ifenprodil was bath-applied, and responses were recorded until ifenprodil block was complete.

Immunoblotting and Protein Quantitation. Hippocampi from littermate mice (6 wk) were solubilized in PBS containing 1% Nonidet P-40, 0.1% SDS, and 1% deoxycholate, they were centrifuged at 20,000 × g_{av} for 20 min, and the supernatants were analyzed by quantitative immunoblotting using ^{125}I-labeled secondary antibodies (36).

Light Microscopy. To quantify dendritic complexity by Sholl analysis, CA1 pyramidal cells were visualized after biocytin delivery during patch-clamp recording (37). Spine quantitations were done on patched neurons filled with dextran-conjugated Alexa-555 (Invitrogen).

EM. Sixty-nanometer-thick sections were obtained from the stratum radiatum of the CA1 region of the hippocampus of two pairs of littermate WT and $NL3^{R451C}$ mutant mice. Sections were poststained with uranyl acetate and lead citrate, and they were examined with a FEI Tecnai transmission electron microscope at 120 kV accelerating voltage; digital images were captured with a 1 × 1 k SIS Morada CCD camera. Quantitative analyses were conducted on digital electron micrographs at magnifications of 18,500 to ~30,000, with average sample areas of 41 μm^2 and 50 images/animal. The number of docked vesicles (defined as vesicles touching the presynaptic plasma membrane), number of vesicles per bouton, PSD length, and bouton and spine area were analyzed using MetaMorph software (Molecular Devices).

Statistical Analyses. Pair-wise comparisons were analyzed by Student *t* test, whereas probability distributions were examined using the Kolmogorov–Smirnov test. All data represent mean ± SEM. For all experiments, the experimenter was blind to genotype throughout data collection and analysis.

ACKNOWLEDGMENTS. This work was supported by National Institute of Mental Health Grant R37 MH052804 (to T.C.S.) and Simons Foundation Grant SF177850 (to T.C.S.).

1. American Psychiatric Association (2000) *Diagnostic Criteria from DSM-IV-TR* (American Psychiatric Association, Washington, DC).
2. Folstein S, Rutter M (1977) Infantile autism: A genetic study of 21 twin pairs. *J Child Psychol Psychiatry* 18:297–321.
3. Persico AM, Bourgeron T (2006) Searching for ways out of the autism maze: Genetic, epigenetic and environmental clues. *Trends Neurosci* 29:349–358.
4. Jamain S, et al. (2003) Mutations of the X-linked genes encoding neuroligins NLGN3 and NLGN4 are associated with autism. *Nat Genet* 34:27–29.
5. Laumonnier F, et al. (2004) X-linked mental retardation and autism are associated with a mutation in the NLGN4 gene, a member of the neuroligin family. *Am J Hum Genet* 74:552–557.
6. Yan J, et al. (2005) Analysis of the neuroligin 3 and 4 genes in autism and other neuropsychiatric patients. *Mol Psychiatry* 10:329–332.
7. Talebizadeh Z, et al. (2006) Novel splice isoforms for NLGN3 and NLGN4 with possible implications in autism. *J Med Genet* 43:e21.
8. Durand CM, et al. (2007) Mutations in the gene encoding the synaptic scaffolding protein SHANK3 are associated with autism spectrum disorders. *Nat Genet* 39:25–27.
9. Moessner R, et al. (2007) Contribution of SHANK3 mutations to autism spectrum disorder. *Am J Hum Genet* 81:1289–1297.
10. Szatmari P, et al. (2007) Mapping autism risk loci using genetic linkage and chromosomal rearrangements. *Nat Genet* 39:319–328.
11. Yan J, et al. (2008) Neurexin 1α structural variants associated with autism. *Neurosci Lett* 438:368–370.
12. Zhang C, et al. (2009) A neuroligin-4 missense mutation associated with autism impairs neuroligin-4 folding and endoplasmic reticulum export. *J Neurosci* 29:10843–10854.
13. Südhof TC (2008) Neuroligins and neurexins link synaptic function to cognitive disease. *Nature* 455:903–911.
14. Betancur C, Sakurai T, Buxbaum JD (2009) The emerging role of synaptic cell-adhesion pathways in the pathogenesis of autism spectrum disorders. *Trends Neurosci* 32:402–412.
15. Tabuchi K, et al. (2007) A neuroligin-3 mutation implicated in autism increases inhibitory synaptic transmission in mice. *Science* 318:71–76.
16. Etherton MR, Tabuchi K, Sharma M, Ko J, Südhof TC (2011) An autism-associated point mutation in the neuroligin cytoplasmic tail selectively impairs AMPA receptor-mediated synaptic transmission in hippocampus. *EMBO J* 30:2908–2919.
17. Varoqueaux F, et al. (2006) Neuroligins determine synapse maturation and function. *Neuron* 51:741–754.
18. Chubykin AA, et al. (2007) Activity-dependent validation of excitatory versus inhibitory synapses by neuroligin-1 versus neuroligin-2. *Neuron* 54:919–931.
19. Gibson JR, Huber KM, Südhof TC (2009) Neuroligin-2 deletion selectively decreases inhibitory synaptic transmission originating from fast-spiking but not from somatostatin-positive interneurons. *J Neurosci* 29:13883–13897.
20. Ko J, et al. (2009) Neuroligin-1 performs neurexin-dependent and neurexin-independent functions in synapse validation. *EMBO J* 28:3244–3255.
21. Kim J, et al. (2008) Neuroligin-1 is required for normal expression of LTP and associative fear memory in the amygdala of adult animals. *Proc Natl Acad Sci USA* 105:9087–9092.
22. Blundell J, et al. (2010) Neuroligin-1 deletion results in impaired spatial memory and increased repetitive behavior. *J Neurosci* 30:2115–2129.
23. Chadman KK, et al. (2008) Minimal aberrant behavioral phenotypes of neuroligin-3 R451C knockin mice. *Autism Res* 1:147–158.
24. Jamain S, et al. (2008) Reduced social interaction and ultrasonic communication in a mouse model of monogenic heritable autism. *Proc Natl Acad Sci USA* 105:1710–1715.
25. Phelps SM, Campbell P, Zheng DJ, Ophir AG (2010) Beating the boojum: Comparative approaches to the neurobiology of social behavior. *Neuropharmacology* 58:17–28.
26. Moy SS, et al. (2004) Sociability and preference for social novelty in five inbred strains: An approach to assess autistic-like behavior in mice. *Genes Brain Behav* 3:287–302.
27. Moy SS, et al. (2007) Mouse behavioral tasks relevant to autism: Phenotypes of 10 inbred strains. *Behav Brain Res* 176:4–20.
28. Crawley JN (2007) Mouse behavioral assays relevant to the symptoms of autism. *Brain Pathol* 17:448–459.
29. Bellone C, Nicoll RA (2007) Rapid bidirectional switching of synaptic NMDA receptors. *Neuron* 55:779–785.
30. Vicini S, et al. (1998) Functional and pharmacological differences between recombinant N-methyl-D-aspartate receptors. *J Neurophysiol* 79:555–566.
31. Cull-Candy SG, Leszkiewicz DN (2004) Role of distinct NMDA receptor subtypes at central synapses. *Sci STKE* 2004:re16.
32. Ichtchenko K, et al. (1995) Neuroligin 1: A splice site-specific ligand for β-neurexins. *Cell* 81:435–443.
33. Ullrich B, Ushkaryov YA, Südhof TC (1995) Cartography of neurexins: More than 1000 isoforms generated by alternative splicing and expressed in distinct subsets of neurons. *Neuron* 14:497–507.
34. Etherton MR, Blaiss CA, Powell CM, Südhof TC (2009) Mouse neurexin-1α deletion causes correlated electrophysiological and behavioral changes consistent with cognitive impairments. *Proc Natl Acad Sci USA* 106:17998–18003.
35. Kaeser PS, et al. (2008) RIM1α phosphorylation at serine-413 by protein kinase A is not required for presynaptic long-term plasticity or learning. *Proc Natl Acad Sci USA* 105:14680–14685.
36. Rosahl TW, et al. (1995) Essential functions of synapsins I and II in synaptic vesicle regulation. *Nature* 375:488–493.
37. Földy C, Lee SH, Morgan RJ, Soltesz I (2010) Regulation of fast-spiking basket cell synapses by the chloride channel ClC-2. *Nat Neurosci* 13:1047–1049.